Journal of Physics: Conference Series **526** (2014) 012006 doi:10.1088/1742-6596/526/1/012006

THz intervalence band antipolaritons

Inuwa A Faragai and Mauro F Pereira

Materials and Engineering Research Institute, Sheffield Hallam University, S1 1WB, Sheffield, UK

E-mail: m.pereira@shu.ac.uk

Abstract. THz polaritons and antipolaritons have strong potential for device applications and are a challenging field of fundamental studies. In this paper, we start from a numerically exact nonequilibrium many body solutions and adjust it to a simplified nonlinear dielectric constant approach to the optical susceptibility. The resulting expression is inserted in the wave equation to describe the coupling of TE-polarized THz radiation with an intervalence band transition in GaAs/$Al_{0.3}Ga_{0.7}$As multiple quantum wells embedded in microcavities. The energy dispersions relations leading to THz polaritons are investigated. Here we focus on the impact of dephasing and scattering processes for different structures and excitation conditions in an inverted medium leading to antipolaritons.

1. Introduction

Intersubband based THz polariton emitters are attracting major research interest [1,2]. The coupling of THz radiation with intersubband transitions in microcavities can lead to further tunability and improved quantum efficiency and may play a major role in future THz materials and devices [3]. In this paper we extend and complement the results of Refs. [4,5] by investigating the influence of dephasing and scattering mechanisms on TE mode, THz antipolaritons in different structures based on GaAs/$Al_{0.3}Ga_{0.7}$As multiple quantum wells. As in the case of conduction band transitions, polaritons [6-8] and antipolaritons [9] can be realized with either absorptive (passive) or gain (inverted) media. However, in contrast to interconduction band transitions, both transverse electric (TE) and transverse magnetic (TM) polarized cavity modes [10] are possible.

2. Mathematical Approach and Model Equations

The input to the dielectric constant used here is obtained by self-consistent evaluation of manybody Nonequilibrium Green's Functions (NGF). The numerical method is summarized as follows. The THz susceptibility χ(ω) is extracted from Keldysh Green's Functions,

$$\left[\hbar\omega - e_{\mu\nu}(k) + i\Gamma_{\mu\nu}\right]\chi_{\nu\mu}(k,\omega) - \Delta n_{\nu\mu}(k)\sum_{\vec{q}\neq\vec{k}}\chi_{\nu\mu}(k',\omega)V^{\nu\mu}_{\vec{q}-\vec{k}} = \wp_{\nu\mu}(k)\Delta n_{\nu\mu}(k). \quad (1)$$

Here $\wp_{\nu\mu}(k)$and $\Delta n_{\nu\mu}(k)$ are the transition dipole moment and the nonequilibrium population difference between hole subbands ν and μ. More details of the renormalized energies $e_{\mu\nu}(k)$, electron-electron scattering $\Gamma_{\mu\nu}$ and Coulomb matrix elements $V^{\nu\mu}_{\vec{q}-\vec{k}}$ are given in Refs. [11-17]. The system is globally out of equilibrium. The holes are thermalized in the upper hole subband (this is the electron-

hole and not the conduction-valence band picture) and the lowest hole band is considered to be empty. The dielectric function is obtained by adjusting the full numerical solution to a Lorentzian, namely

$$\varepsilon(\omega) = \varepsilon_b + 4\pi\lambda\chi(\omega) = 1 - \frac{\lambda}{\varepsilon_b}\sum_{\mu\nu}\frac{\Lambda_{\mu\nu}}{\omega-\omega_{\mu\nu}+i\gamma_{\mu\nu}} - \frac{\Lambda_{\mu\nu}}{\omega+\omega_{\mu\nu}+i\gamma_{\mu\nu}} \quad (2)$$

$\chi(\omega)$ is the total optical susceptibility, ε_b, ω, and $\omega_{\mu\nu}$ are background dielectric constant, photons and transition frequencies between subbands $\mu \neq \nu$ respectively. The constant λ is given by $\lambda = N_w \frac{L_c}{L_w}$ [14], where N_w is the number of QWs, L_w and L_c denote respectively the QW and cavity core lengths. Here $\gamma_{\mu\nu}$ is the dephasing term, while $\Lambda_{\mu\nu}$ is due to dipole coupling and measures the oscillator strength of the transition. The dispersion relations shown in Fig.2 are obtaining by substituting Eq. (2) into Maxwells' equations [9,10]. Introducing $y = \frac{\omega}{\omega_o}$, $\Omega_c = \frac{\omega_c}{\omega_0} = \frac{c\pi}{\omega_o L_c}\left(\frac{1}{\varepsilon_b}\right)^{\frac{1}{2}}$ for the cavity resonance and ω_o , the reference resonance frequency (for one transition between subbands 1 and 2, $\omega_0 = \omega_{12}$ ε_r and ε_i , we obtain the dispersion relation

$$\sin\theta_i = \left(\frac{\varepsilon_b}{\varepsilon_s}\right)^{\frac{1}{2}}\sqrt{1-\lambda\Phi-\frac{\Omega_c^2}{y^2}} \quad , \Phi = \sum_{\mu\nu}\frac{\Delta_{\mu\nu}(y-\Omega_{\mu\nu})}{(y-\Omega_{\mu\nu})^2+\Gamma^2} - \frac{\Delta_{\mu\nu}(y+\Omega_c)}{(y+\Omega_c)^2+\Gamma^2}, \Delta_{\mu\nu} = \frac{\Lambda_{\mu\nu}}{\varepsilon_b\omega_o} \text{ and } \Gamma = \frac{\gamma_{\mu\nu}}{\omega_o}. \quad (3)$$

The geometry considered in this work is shown in Fig. 1. In order to ensure that incident light reaches the sample in the cavity with a suitable incidence angle, a prism made of a high refractive material is placed on top of the sample.

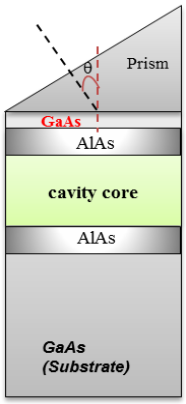

Figure 1. Sample structure. Light is confined through total internal reflection by low refractive index AlAs layers below and above the cavity core, which contains 170 GaAs quantum wells, each separated by 150nm $Al_{0.3}Ga_{0.7}As$ barrier except the last top barrier layer which was set to 250nm and these lead to cavity lengths L_C equal to 26.6μm and 28.5μm for the 5nm and 10nm MQW structures respectively. The top and bottom layers of AlAs are both set to 1300 nm and then completed the sample with a top 5nm GaAs to avoid AlAs oxidation due to air interface. The corresponding cavity parameters are: cavity resonances ω_c = 7.3579meV / 6.8568meV; background dielectric constant ε_b = 10.0117 / 10.0392 and the effective medium constant λ = 0.0319 / 0.0596 for 5nm / 10nm MQW samples.

2. Numerical Results and Discussion

THz antipolaritons due to interacting TE- polarized cavity modes and intervalence band transitions in the gain regime are shown next for two different samples, in which the cavities have either 10nm or 5nm GaAs/$Al_{0.3}Ga_{0.7}As$ MQWs. Figure 2 shows the influence of dephasing 'γ' and the effect of changing the carrier density 'ΔN', on the THz intervalence band antipolariton dispersions for a sample following the geometric structure shown in Fig. 1 for 5nm ((a) and (b)) and 10nm ((c) and (d)) MQWs respectively. Since the lowest band is assumed to be empty, this also corresponds to the population difference. $\mu, \nu = 1,2$ denote respectively the first and second subbands. $\Lambda_{\mu\nu}$ and $\omega_{\mu\nu}$ are obtained by adjusting the full numerical manybody expression to the Lorentzian approximation in Eq. 2. The increasing dephading for fixed carrier densities simulates time resolved experiments in which the onset of dephasing can be monitored. The dephasing increases from the outer curves towards the centre. Analogously to the interband exciton [18] and the TM mode inter-conduction band cases [19],

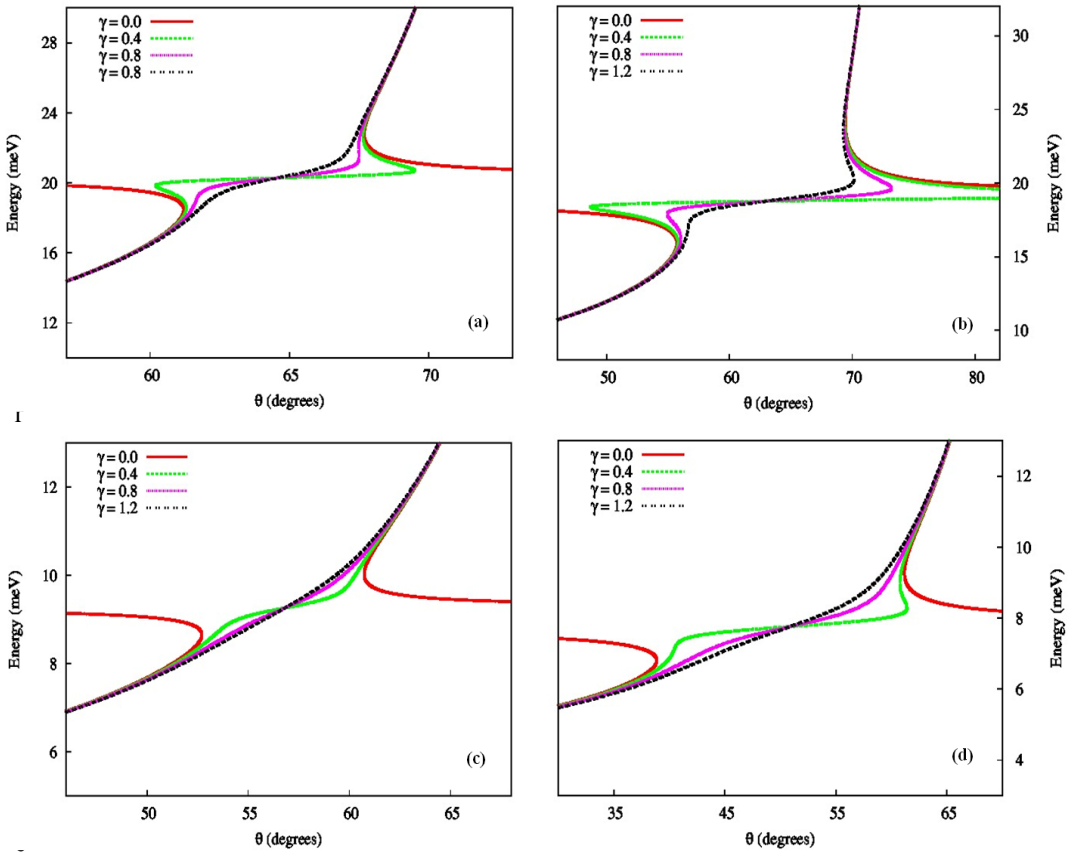

Figure 2. THz intervalence band antipolaritons due to coupling of a TE polarized cavity mode and intervalence band excitations: (a) Lw = 5nm, $\Delta N = 1.0\times10^{11}$ cm^{-2} $\Lambda_{\mu\nu}$ = -8.4634 meV, $\omega_{\mu\nu}$ = 20.2753. (b) Lw = 5nm, $\Delta N = 4.0 \times 10^{11}$ cm^{-2}, $\Lambda_{\mu\nu}$ = -32.7163 meV, $\omega_{\mu\nu}$ =18.7734 me. (c) Lw = 10nm, $\Delta N = 1.0\times10^{11}$ cm^{-2}, $\Lambda_{\mu\nu}$ = -25.5945, $\omega_{\mu\nu}$ = 7.7596. (d) Lw = 10nm, $\Delta N = 4.0 \times 10^{11}$ cm^{-2}, $\Lambda_{\mu\nu}$ = -25.5945, $\omega_{\mu\nu}$ = 7.7596.

Note that the 5 nm MQWs have transitions with larger transition energies than the 10 nm MQWs so for the same dephasing, the antipolariton features are stronger. Compare the dashed lines in both cases. For larger densities, the absolute value of the longitudinal-transverse (LT) splitting $\Delta_{\mu\nu}$ increases. This increased oscillator strength leads to a stronger separation of the two branches. Note however the interplay of larger quantum well width (and thus larger λ factor) and larger oscillator strengths that make the branch separation comparable for the same density. In other words, even though $\Delta_{\mu\nu}$ is larger for the 5 nm MQWs, due to better electronic overlap, λ is larger in the structure containing 10 nm MQWs, roughly equilibrating the effect. This study further suggests that samples with different well widths in the active region might lead to larger tunability (see the different energy ranges) in applications where the antipolariton coupling might be used.

In we have investigated the interaction of TE Mode THz radiation and intervalence band transitions in quantum well gain media. This can lead to interesting THz based devices based on TE modes in contrast with inter-conduction band transitions that only couple to TM polarized radiation. A Nonequilibrium Many Body Approach for the optical response beyond the Hartree-Fock approximation is used as input to the effective dielectric function formalism for the polariton problem. The energy dispersions relations in the THz range are obtained by adjusting the full numerical solutions to simple analytical expressions to improve clarity, allowing a broad audience to investigate similar phenomena. The method allows to combine predictive microscopic optical responses with a simple dielectric model for the cavity leading to a powerful design tool for THz polaritonics.

Acknowledgements
The authors acknowledge support from COST ACTIONs MP1204 and BM1205. I.A. Faragai's research is supported by the KUST-Wudil under TETFUND, Nigeria

References

[1] S. De Liberato, C. Ciuti and C. C. Phillips, Terahertz lasing from intersubband polariton-polariton scattering in asymmetric quantum wells, Phy. Rev. B. 87, 241304(R) (2013).
[2] M. Geiser, G. Scalari, F. Castellano, M. Beck and J. Faist, Room temperature terahertz polariton emitter Applied Physics Letters 101, 141118 (2012).
[3] M.F. Pereira, TERA-MIR radiation: materials, generation, detection and applications, Opt Quant Electron 46, pp. 491–493 (2014).
[4] I. A. Faragai and M. F. Pereira, Interaction of valence band excitations and terahertz TE-polarized cavity modes, Optical and Quantum Electronics, Opt Quant Electron 46, pp. 527–531, (2014).
[5] M.F. Pereira and I.A. Faragai, Coupling of THz with intervalence band transitions in microcavities, Optics Express, Vol. 22, Issue 3, pp. 3439-3446 (2014).
[6] D. Dini, R. Köhler, A. Tredicucci, G. Biasiol, L. Sorba, and F. Beltram, "Microcavity Polariton Splitting of Intersubband Transitions", Phys. Rev. Lett. 90, 116401 (2003).
[7] A. A. Anappara, A. Tredicucci and F. Beltram, Cavity polaritons from excited-subband transitions, App. Phys. Lett., 91, 231118 (2007).
[8] S. de Liberato,and C. Ciutti, Stimulated scattering and lasing of intersubband cavity polaritons, Phys. Rev. Lett. 102, 136403 (2009)
[9] M. F. Pereira Jr. Intersubband antipolaritons: Microscopic approach, Phys. Rev. B 75, 195301 (2007).
[10] M.F. Pereira Jr. and H. Wenzel, Interplay of Coulomb and nonparabolicity effects in the intersubband absorption of electrons and holes in quantum wells, Phys. Rev. B70, 205331 (2004
[11] M. F. Pereira Jr., Intervalence transverse-electric mode terahertz lasing without population inversion, Phys. Rev. B 78, 245305 (2008).
[12] T. Schmielau and M.F. Pereira Jr., Nonequilibrium many body theory for quantum transport in terahertz quantum cascade lasers, Appl. Phys. Lett. 95, 231111 (2009).
[13] T. Schmielau and M.F. Pereira, Impact of momentum dependent matrix elements on scattering effects in quantum cascade lasers, physica status solidi b 246, 329 (2009).
[14] M.F. Pereira Jr, R. Nelander, A. Wacker, D.G. Revin, M.R.Soulby, L.R. Wilson, J.W. Cockburn, A.B. Krysa, J.S. Roberts, and R.J. Airey, Characterization of Intersubband Devices Combining a Nonequilibrium Many Body Theory with Transmission Spectroscopy Experiments, Journal of Materials Science: Materials in Electronics 18, 689 (2007).
[15] M.F. Pereira Jr, R. Nelander, A. Wacker, D.G. Revin, M.R.Soulby, L.R. Wilson, J.W. Cockburn, A.B. Krysa, J.S. Roberts, and R.J. Airey, "Characterization of Intersubband Devices Combining a Nonequilibrium Many Body Theory with Transmission Spectroscopy Experiments", Journal of Materials Science: Materials in Electronics 18, 689 (2007).
[16] M. F. Pereira and S. Tomić, Intersubband gain without global inversion through dilute nitride band engineering, Appl. Phys. Lett. 98, 061101 (2011)
[17] M.F. Pereira Jr., Microscopic approach for intersubband-based thermophotovoltaic structures in the THz and Mid Infrared, JOSA B Vol. 28, Iss. 8, pp. 2014–2017 (2011).
[18] A. Quattropani, W. Czaja, Physica Scripta T29, 162 (1989)
[19] M.F. Pereira, The influence of dephasing in the coupling of light with intersubband transitions, Microelectronics Journal 40, 841 (2009).